Supplement of Atmos. Meas. Tech., 15, 2077–2098, 2022
https://doi.org/10.5194/amt-15-2077-2022-supplement

Atmospheric Measurement Techniques
Open Access
EGU

Supplement of

Enhancing MAX-DOAS atmospheric state retrievals by multispectral polarimetry – studies using synthetic data

Jan-Lukas Tirpitz et al.

Correspondence to: Jan-Lukas Tirpitz (jan-lukas.tirpitz@airyx.de)

S1 Dependence of light path on the polariser angle

A convenient concept to encompass the complex light path geometries in MAX-DOAS applications is the airmass-factor (AMF), defined as $A_s(\lambda,\Omega) = S_s(\lambda,\Omega)/V_s$, in terms of the vertical column density V_s and the SCD $S_s(\lambda,\Omega)$ for trace gas s. We further define the "AMF eccentricity"

$$\epsilon_s = 2\frac{\max_\delta(A_s) - \min_\delta(A_s)}{\max_\delta(A_s) + \min_\delta(A_s)}, \tag{1}$$

which quantifies the relative change in AMF obtained with a polariser in a distinct viewing direction. Figure S1 shows values of the AMF eccentricities ϵ over the sky hemisphere; these were simulated for a Rayleigh atmosphere through application of the RAPSODI forward model described in Section 5.3. The largest eccentricities occur in the Vis spectral range, for species with comparably large scale height values (like O_4) and in directions of strong polarisation (compare skylight polarisation patterns e.g. by Emde et al., 2010).

It is also interesting to investigate the box-airmass-factors (BAMFs) A_l, which describe the ratio of slant and vertical light paths through a single homogenous model layer l. For small trace gas optical thicknesses, they can be calculated according to

$$A_l = -\frac{1}{I}\frac{dI}{d\tau_l^{\text{abs}}},, \tag{2}$$

which is just the normalised sensitivity of the simulated radiance I with respect to the layer's vertical absorption optical thickness τ_l^{abs}. Figure S2 shows the BAMFs for a viewing direction having particularly large O_4 AMF eccentricity.

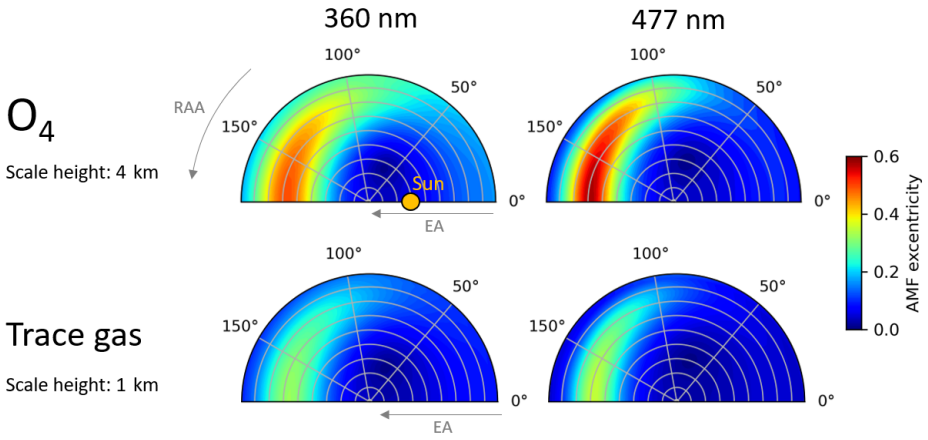

Figure S1. Eccentricity of the AMF modelled over the sky hemisphere for a Rayleigh atmosphere in two major O_4 absorption bands at 360 and 477 nm, respectively. The upper row shows AMFs for O_4, while the bottom plots show AMFs for an arbitrary trace gas confined to lower altitudes (exponential profile with scale height of 1 km).

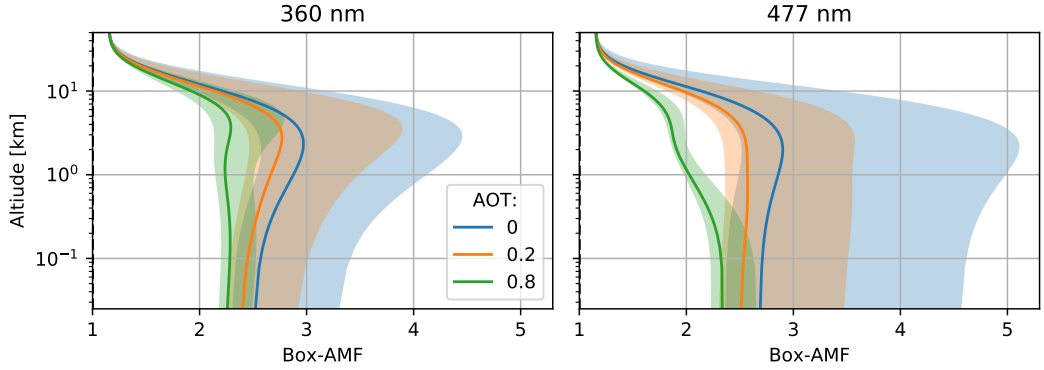

Figure S2. BAMFs at 360 and 477 nm, respectively, for different AOTs. Aerosol properties according to Table 4 in the main text were assumed. Lines show conventional "non-polarimetric" BAMFs, while shaded areas indicate the variation with polariser angle. The assumed geometry is RAA = 180°, SZA = 30° and EA = 30°, a configuration for which these variations are particularly large (compare Figure S1).

S2 Aerosol properties

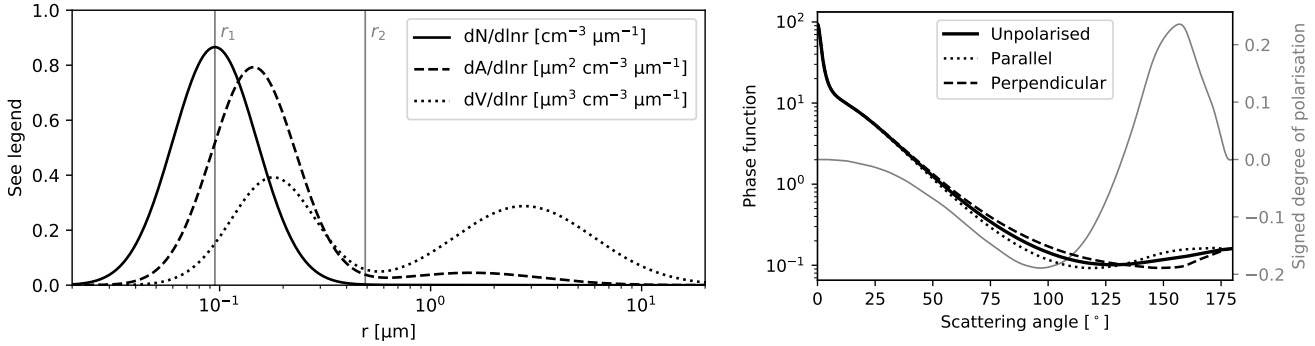

Figure S3. Left panel: the assumed Mie aerosol size distribution in terms of normalised particle number (N), particle surface area (A) and particle volume (V). Precise values of the corresponding parameters are given in Table 4 of the main text. Right panel: Illustration of the corresponding scattering matrix $\mathbf{P}$ at $\lambda = 400\,\mathrm{nm}$. Phase functions are shown for unpolarised incoming light (matrix element P_{11}), as well as for polarisations parallel ($P_{11} + P_{12}$) and perpendicular ($P_{11} - P_{12}$) to the scattering plane. Grey lines and scales indicate the DOLP after a single scattering event of initially unpolarised light (P_{12}/P_{11}). This has a definite sign: positive and negative values indicate emerging polarisations perpendicular and parallel to the scattering plane, respectively.

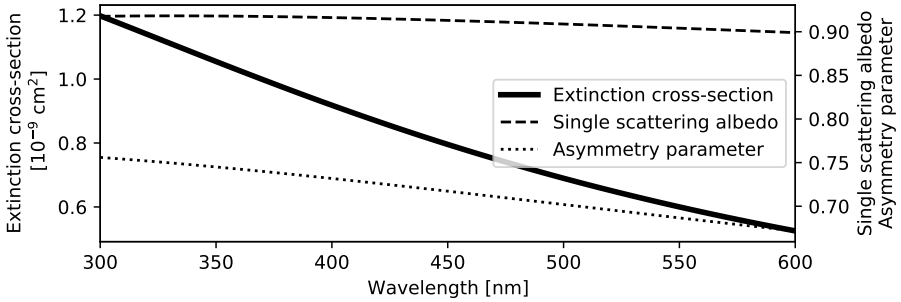

Figure S4. Bulk aerosol optical properties for aerosol with microphysical properties as defined in Table 4 in the main text.

S3 Information content analysis

Table S1. Same as Table 6 in the main text, but for a reduced state vector $\mathbf{x}$ in which the profiles are retrieved, but surface and aerosol properties are fixed to their true values as given in Table 4 in the main text.

Measurement mode					Total	Profiles		
Band	S	P	A	I		c_{aer}	c_{HCHO}	c_{NO_2}
UV	✗	✗	✗	✗	7.2	2.29	1.93	2.97
UV	✓	✗	✗	✗	7.2	2.54	1.88	2.77
UV	✓	✓	✗	✗	8.7	3.18	2.29	3.23
Vis	✗	✗	✗	✗	5.5	2.56	0.0	2.89
Vis	✓	✗	✗	✗	5.5	2.78	0.0	2.68
Vis	✓	✓	✗	✗	6.6	3.52	0.0	3.09
Multi	✓	✗	✗	✗	8.2	3.24	1.9	3.1
Multi	✗	✓	✗	✗	9.8	3.67	2.34	3.77
Multi	✓	✓	✗	✗	9.9	3.99	2.31	3.59
Multi	✓	✗	✓	✗	9.2	3.71	2.13	3.41
Multi	✓	✓	✓	✗	10.9	4.38	2.58	3.92
Multi	✓	✗	✗	✓	8.6	3.58	1.9	3.11
Multi	✓	✓	✓	✓	10.9	4.43	2.58	3.92
					75	25	25	25

Table S2. Similar to Table 6 in the main text, but with DOFS obtained with partially included polarimetric information: "Multi-S-P (dSCDs)" assumes that only polarimetric dSCDs are included in $\hat{\mathbf{y}}$, and "Multi-S-P (dSOTs)" assumes that only polarimetric dSOTs are included.

Mode	Total	Profiles			Surface	Aerosol properties								
Band		c_{aer}	c_{HCHO}	c_{NO_2}	ω_{surf}	r_1	r_2	σ_1	σ_2	$\Re n_1$	$\Re n_2$	$\Im n_1$	$\Im n_2$	f
Multi-S	13.5	1.99	0.44	1.77	1.32	0.15	2.77	0.01	2.89	0.73	0.07	0.51	0.16	0.67
Multi-S-P (dSCDs)	17.8	3.04	0.61	2.16	1.83	0.26	3.06	0.06	3.4	0.83	0.1	0.67	0.24	1.56
Multi-S-P (dSOTs)	18.8	2.5	0.56	1.83	2.24	0.41	5.1	0.1	2.95	0.8	0.09	0.65	0.18	1.37
Multi-S-P	21.9	3.24	0.65	2.21	2.54	0.5	5.22	0.15	3.43	0.87	0.11	0.75	0.26	1.95
	110	25	25	25	6	1	1	1	1	6	6	6	6	1

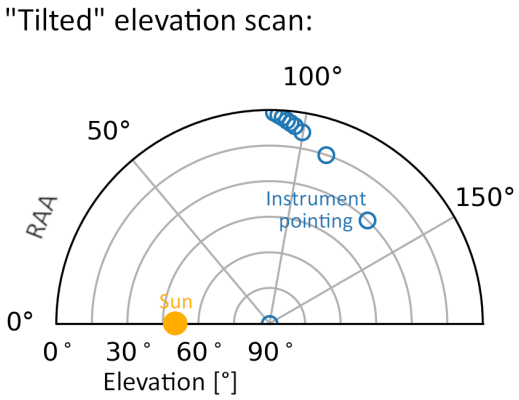

Figure S5. Viewing directions for a tilted elevation scan. For a given EA sequence and SZA, the RAA is chosen to realise a single scattering angle as close to 90° as possible. In this example the EA sequence according to Table 3 in the main text and an SZA of 40° was assumed.

S4 Retrieval results

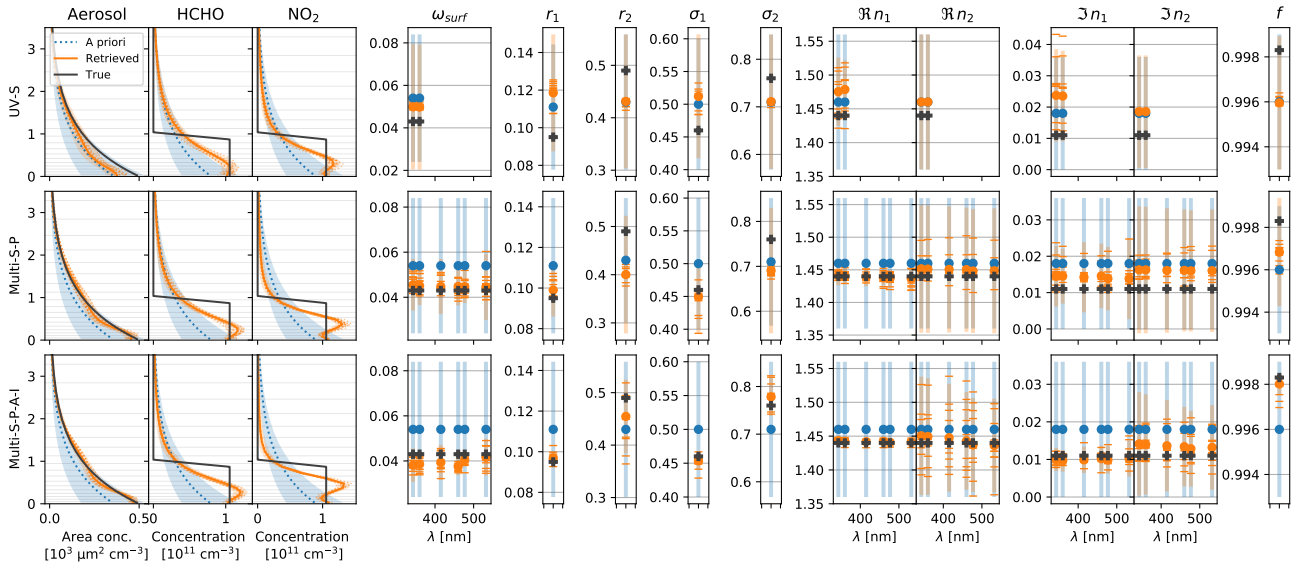

Figure S6. Retrieval results for the Aer1-TG7 scenario. Sub-plot rows show different measurement modes (see captions on the left). The first three subplot columns show profiles with altitudes in [km] on the y-axis. Remaining columns show values (y-axis) for other state vector elements (see captions at the top), sometimes for different wavelengths (x-axis). Blue lines and symbols indicate a priori values, dark grey lines and crosses show true values. Thick orange lines and circles indicate results for a noiseless retrieval, while thin lines and dashes show results of the ten retrievals with random noise added to the observations. Transparent areas and bars indicate uncertainties.

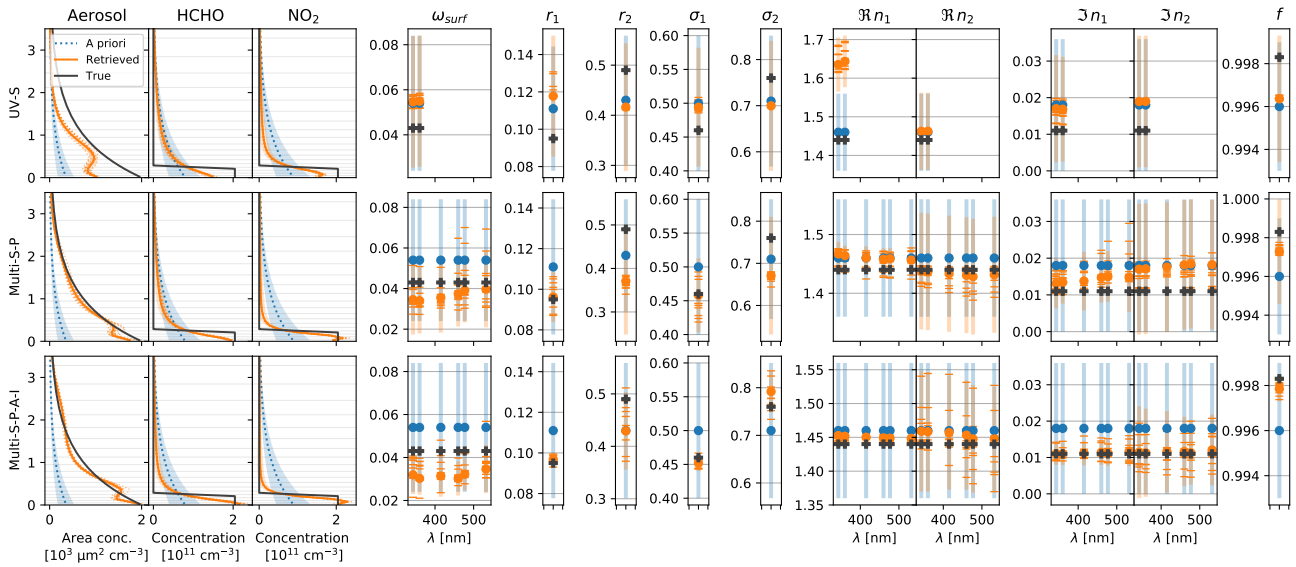

Figure S7. Retrieval results for the Aer2-TG5 scenario. The caption of Figure S6 applies.

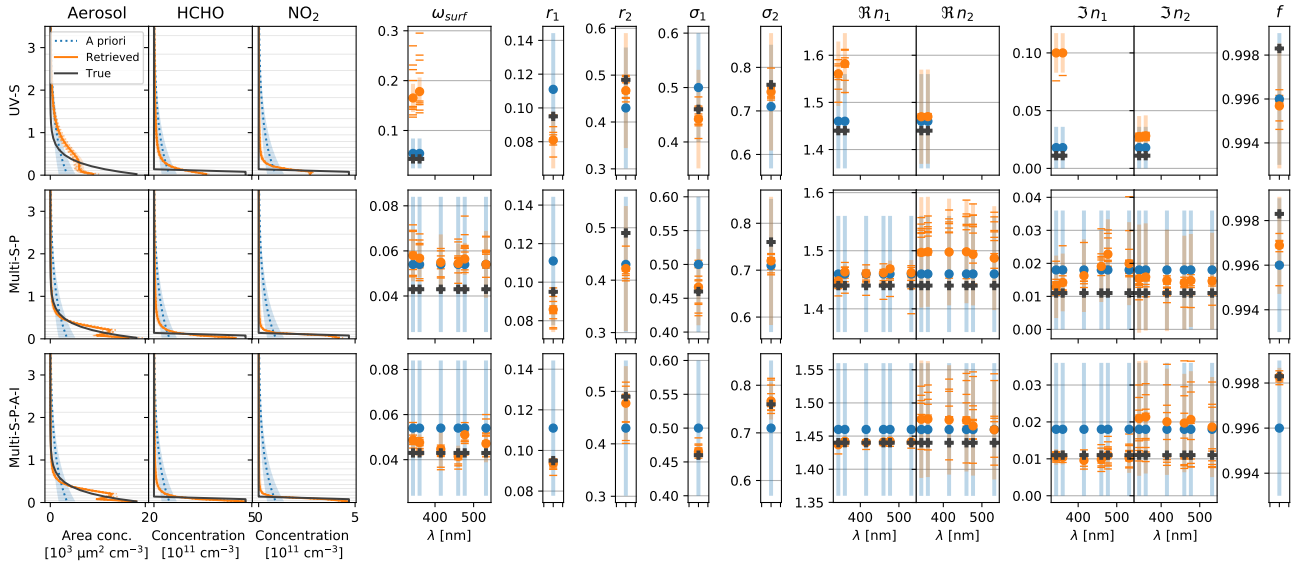

Figure S8. Retrieval results for the Aer3-TG4 scenario. The caption of Figure S6 applies.

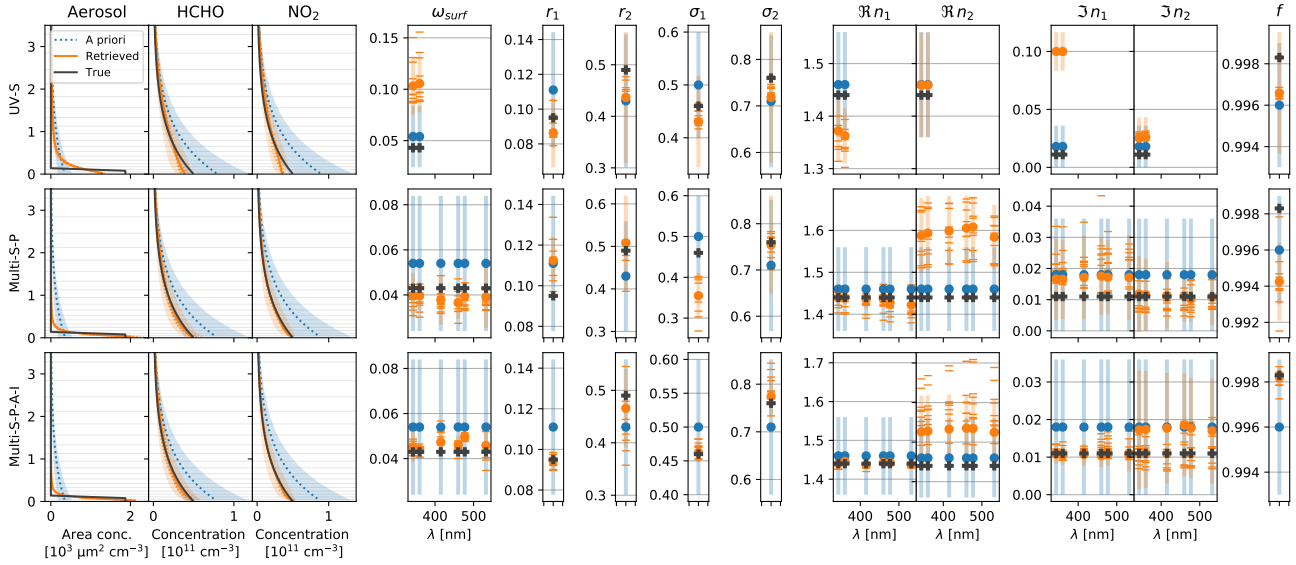

Figure S9. Retrieval results for the Aer4-TG1 scenario. The caption of Figure S6 applies.

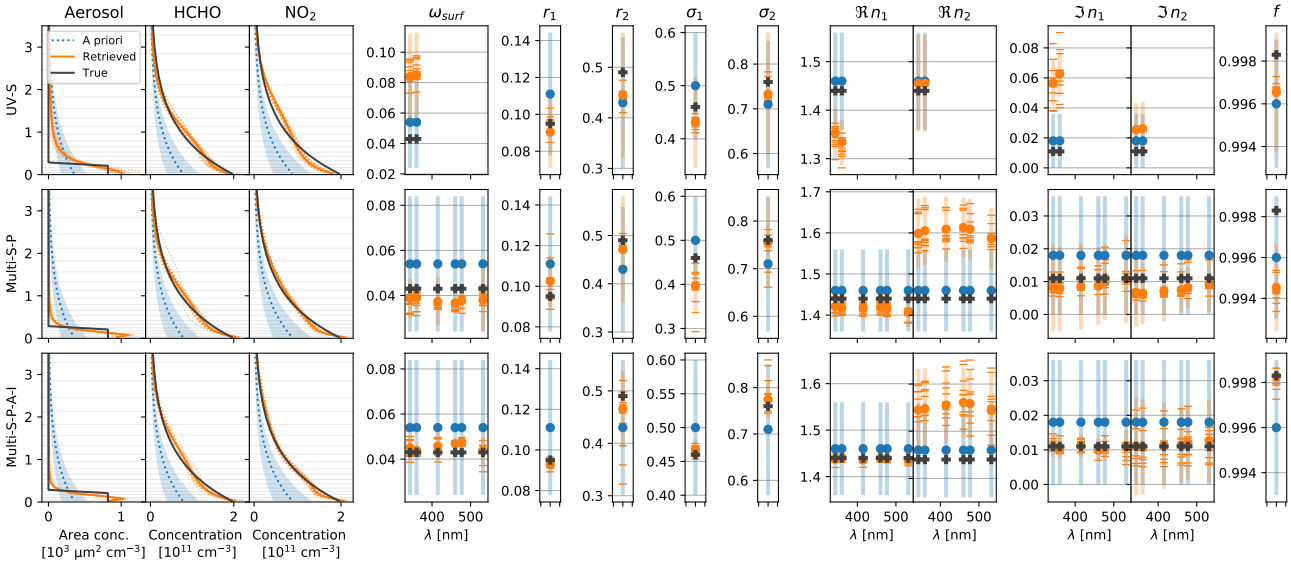

Figure S10. Retrieval results for the Aer5-TG2 scenario. The caption of Figure S6 applies.

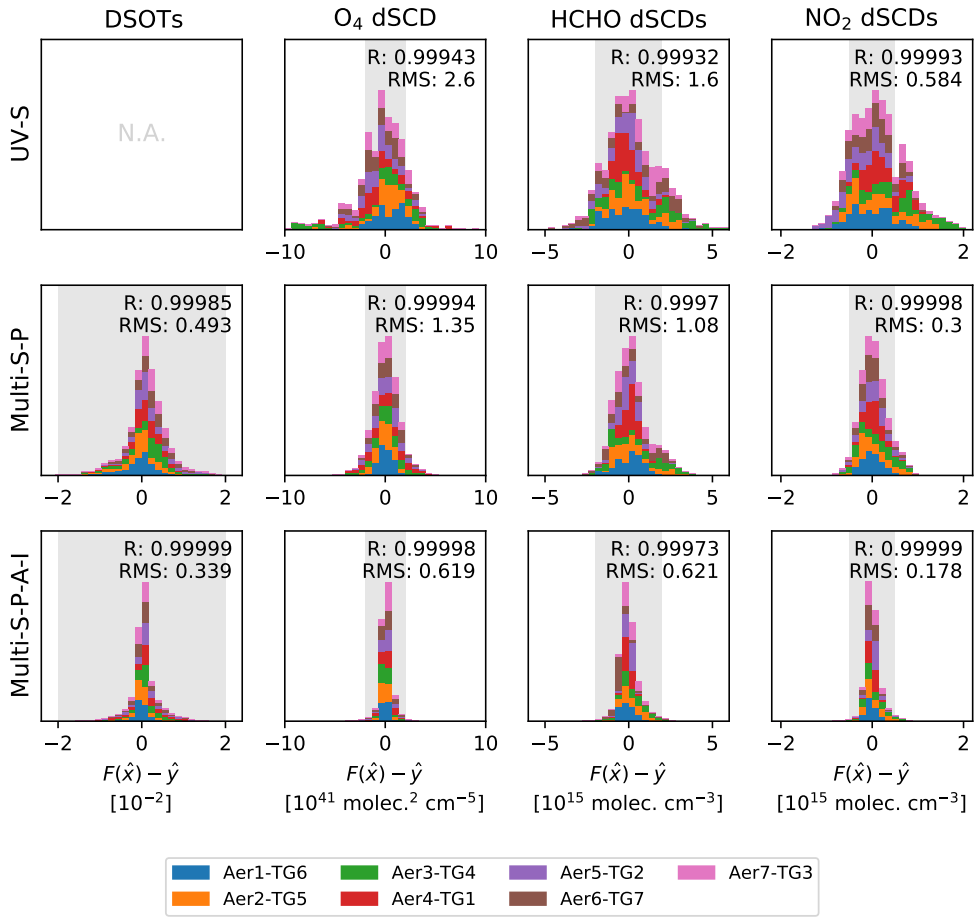

Figure S11. Deviations between the input observations $\hat{\mathbf{y}}$ and the modelled observations $\mathbf{F}(\hat{\mathbf{x}})$ for the retrieved states $\hat{\mathbf{x}}$, illustrating the quality of the convergence. Sub-plot columns show different kinds of observations. Sub-plot rows represent different measurement modes. Y-axes are occurrences in arbitrary units. Grey-shaded areas indicate the assumed measurement uncertainties according to Table 1. RMS values are given in the horizontal axes' units.

S5 Results with increased noise for polarimetric dSCDs

Table S3. Obtained DOFS for the Mie aerosol case. This table is similar to Table 6, but with the noise of polarimetric dSCDs increased by a factor of $\sqrt{6}$.

Measurement mode					Total	Profiles			Surface	Aerosol properties								
Band	S	P	A	I		c_{aer}	c_{HCHO}	c_{NO_2}	ω_{surf}	r_1	r_2	σ_1	σ_2	$\Re n_1$	$\Re n_2$	$\Im n_1$	$\Im n_2$	f
UV	✗	✗	✗	✗	8.6	1.21	1.93	2.97	0.17	0.65	0.04	0.21	0.09	0.81	0.0	0.33	0.02	0.21
UV	✓	✗	✗	✗	8.9	1.51	1.76	2.59	0.24	0.68	0.05	0.24	0.11	1.01	0.0	0.43	0.03	0.24
UV	✓	✓	✗	✗	9.9	1.93	1.6	2.49	0.52	0.71	0.06	0.35	0.11	1.06	0.0	0.65	0.05	0.34
Vis	✗	✗	✗	✗	7.2	1.3	0.0	2.89	0.18	0.65	0.05	0.36	0.09	0.82	0.0	0.47	0.06	0.31
Vis	✓	✗	✗	✗	7.5	1.52	0.0	2.31	0.26	0.66	0.05	0.37	0.1	1.26	0.0	0.57	0.08	0.33
Vis	✓	✓	✗	✗	9.1	2.11	0.0	2.31	0.59	0.7	0.06	0.5	0.11	1.38	0.03	0.69	0.17	0.48
Multi	✓	✗	✗	✗	13.5	1.99	1.77	2.89	0.67	0.73	0.07	0.51	0.16	2.77	0.01	1.32	0.15	0.44
Multi	✗	✓	✗	✗	17.7	2.28	1.72	3.1	1.25	0.79	0.08	0.62	0.15	4.87	0.1	1.89	0.36	0.53
Multi	✓	✓	✗	✗	18.5	2.56	1.65	2.81	1.46	0.81	0.08	0.64	0.16	5.09	0.11	2.18	0.41	0.55
Multi	✓	✗	✓	✗	16.4	2.39	1.86	3.05	1.19	0.8	0.18	0.69	0.51	2.89	0.02	1.74	0.22	0.87
Multi	✓	✓	✓	✗	22.7	2.98	1.75	2.97	2.24	0.9	0.2	0.86	0.52	5.53	0.28	2.78	0.76	0.9
Multi	✓	✗	✗	✓	20.8	2.46	1.83	2.99	1.62	0.81	0.11	0.69	0.24	5.15	0.04	3.86	0.45	0.55
Multi	✓	✓	✓	✓	29.2	3.27	1.78	3.02	3.45	0.98	0.69	0.97	0.93	5.91	0.8	5.02	1.35	0.98
					110	25	25	25	6	1	1	1	1	6	6	6	6	1

Table S4. Obtained DOFS for the the case of a reduced state vector $\mathbf{x}$: only profiles are retrieved, whereas surface and aerosol properties are fixed to the true values as given in Table 4 in the main text. Table is similar to Table S1 but with the noise of polarimetric dSCDs increased by a factor of $\sqrt{6}$.

Measurement mode					Total	Profiles		
Band	S	P	A	I		c_{aer}	c_{HCHO}	c_{NO_2}
UV	✗	✗	✗	✗	7.2	2.29	1.93	2.97
UV	✓	✗	✗	✗	7.2	2.54	1.88	2.77
UV	✓	✓	✗	✗	6.8	2.56	1.68	2.6
Vis	✗	✗	✗	✗	5.5	2.56	0.0	2.89
Vis	✓	✗	✗	✗	5.5	2.78	0.0	2.68
Vis	✓	✓	✗	✗	5.4	2.84	0.0	2.56
Multi	✓	✗	✗	✗	8.2	3.24	1.9	3.1
Multi	✗	✓	✗	✗	7.8	2.99	1.72	3.1
Multi	✓	✓	✗	✗	7.9	3.26	1.7	2.93
Multi	✓	✗	✓	✗	8.7	3.44	1.99	3.23
Multi	✓	✓	✓	✗	8.3	3.45	1.79	3.05
Multi	✓	✗	✗	✓	8.6	3.58	1.9	3.11
Multi	✓	✓	✓	✓	8.4	3.55	1.79	3.06
					75	25	25	25

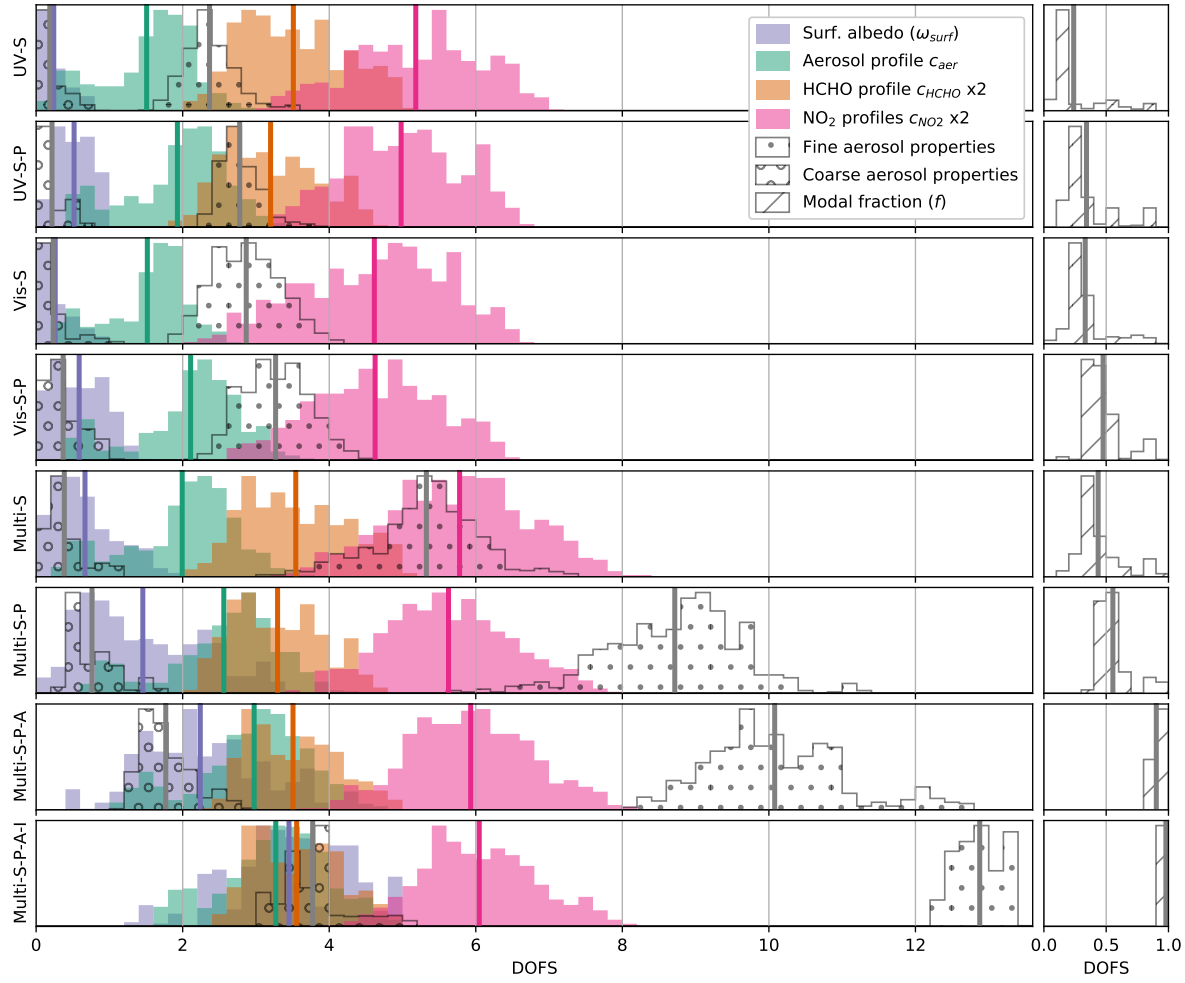

Figure S12. Visualisation of Table S3. This figure is similar to Figure 3 in the main text but with the noise of polarimetric dSCDs increased by a factor of $\sqrt{6}$.

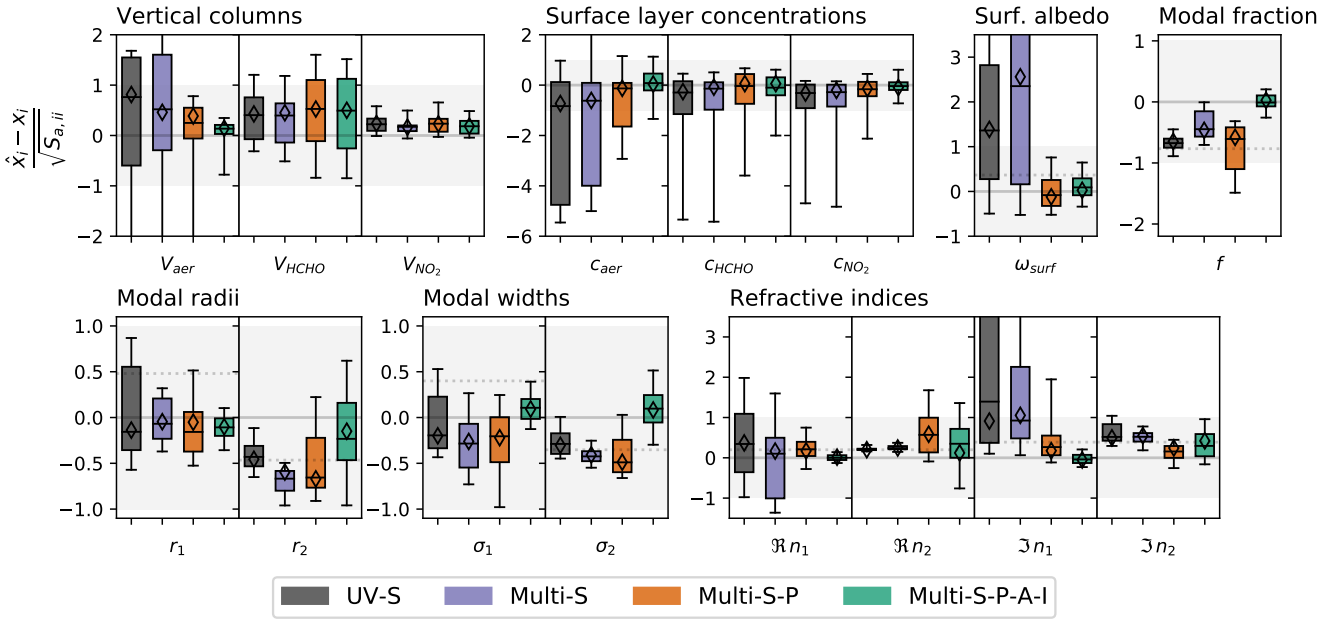

Figure S13. Statistical representation of all retrieval results. This figure is similar to Figure 11 in the main text but with the noise of polarimetric dSCDs increased by a factor of $\sqrt{6}$.

S6 Effect of spatio-temporal variability in atmospheric composition

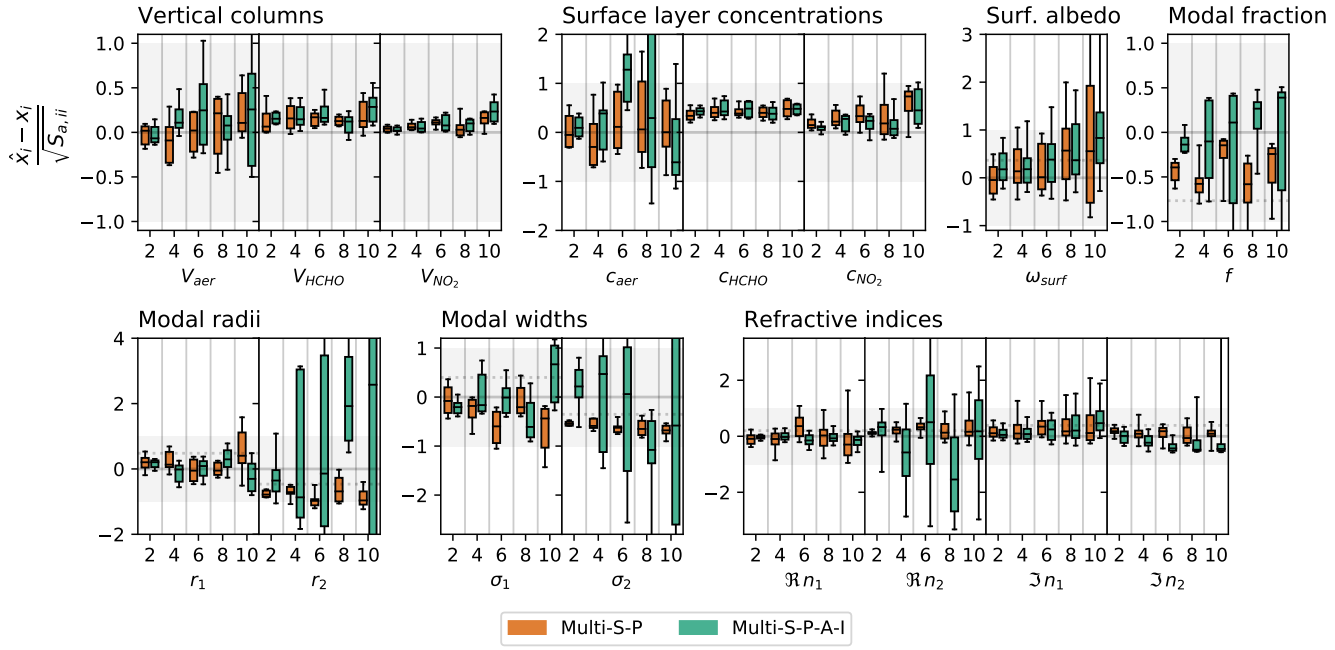

Figure S14. Statistical representation of the retrieval results for the Multi-S-P and the Multi-S-P-A-I modes, with inhomogeneity noises of different magnitudes. The x-axes of each subplot indicates the noise magnitude in percent. The figure is organised in a similar manner to Figure 11 in the main text.

S7 Impact of a priori covariance

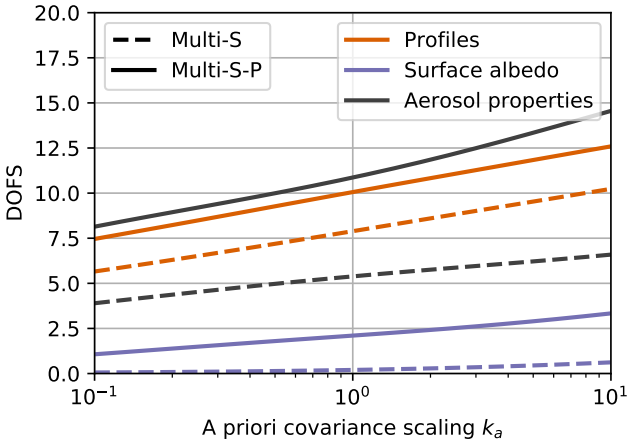

Figure S15. Investigation on the impact of the choice of $\mathbf{S}_a$ on the DOFS reported in this study. The figure shows the behaviour of the DOFS for various measurement modes and parameter subgroups, when $\mathbf{S_a}$ is scaled by a factor k_a. Calculations were performed for $\theta = 60°$, $\phi = 90°$, and Aer1-TG1 profiles.

References

Emde, C., Buras, R., Mayer, B., and Blumthaler, M.: The impact of aerosols on polarized sky radiance: model development, validation, and applications, Atmospheric Chemistry and Physics, 10, 383–396, https://doi.org/10.5194/acp-10-383-2010, https://acp.copernicus.org/articles/10/383/2010/, 2010.